Quantum critical behavior of a three-dimensional superfluid-Mott glass transition

Jack Crewse, Cameron Lerch, and Thomas Vojta
Department of Physics, Missouri University of Science & Technology, Rolla, Missouri 65409, USA

(Received 31 May 2018; revised manuscript received 23 July 2018; published 22 August 2018)

The superfluid to insulator quantum phase transition of a three-dimensional particle-hole symmetric system of disordered bosons is studied. To this end, a site-diluted quantum rotor Hamiltonian is mapped onto a classical (3+1)-dimensional XY model with columnar disorder and analyzed by means of large-scale Monte Carlo simulations. The superfluid-Mott insulator transition of the clean, undiluted system is in the four-dimensional XY universality class and shows mean-field critical behavior with logarithmic corrections. The clean correlation length exponent $\nu = 1/2$ violates the Harris criterion, indicating that disorder must be a relevant perturbation. For nonzero dilutions below the lattice percolation threshold of $p_c = 0.688\,392$, our simulations yield conventional power-law critical behavior with dilution-independent critical exponents $z = 1.67(6)$, $\nu = 0.90(5)$, $\beta/\nu = 1.09(3)$, and $\gamma/\nu = 2.50(3)$. The critical behavior of the transition across the lattice percolation threshold is controlled by the classical percolation exponents. Our results are discussed in the context of a classification of disordered quantum phase transitions, as well as experiments in superfluids, superconductors, and magnetic systems.

DOI: 10.1103/PhysRevB.98.054514

I. INTRODUCTION

Models of disordered and interacting bosons can be employed to describe a wide variety of physical phenomena, including helium absorbed in porous media [1,2], superconducting thin films [3,4], Josephson junction arrays [5,6], ultracold atoms in disordered optical lattices [7–9], and certain disordered quantum magnets [10–14].

It is well established [15–17] that the Mott insulating and superfluid phases of these models are always separated by an insulating "glass" phase in which rare large regions of local superfluid order (superfluid "puddles") coexist with the insulating bulk. The glass phase thus acts as a Griffiths phase [18–21] of the superfluid-Mott insulator quantum phase transition.

The nature of the glassy intermediate phase depends on the qualitative properties of the disorder. For generic disorder (realized, e.g., via a random potential for the bosons), it is the so-called Bose glass, a compressible gapless insulator. The zero-temperature phase transition between the superfluid and Bose glass ground states has recently reattracted a great deal of attention as new analytical [22], numerical [23–27], and experimental [12,13,28] work has challenged the scaling relation [16,17] $z = d$ between the dynamical exponent z and the space dimensionality d as well as the value of the crossover exponent ϕ that governs the shape of the finite-temperature phase boundary.

If the system is particle-hole symmetric even in the presence of disorder, the intermediate phase between superfluid and Mott insulator is not a Bose glass but the *incompressible* gapless Mott glass [29,30]. (This state is sometimes called random-rod glass because in a classical representation the disorder takes the form of infinitely long parallel rods.) The zero-temperature phase transition between the superfluid and Mott glass ground states has received less attention than the Bose glass transition, perhaps because in some experimental applications the condition of exact particle-hole symmetry is hard to realize and requires fine tuning. Note, however, that the particle-hole symmetry appears naturally in magnetic realizations of disordered boson physics due to the up-down symmetry of the spin Hamiltonian in the absence of an external magnetic field.

We have recently determined the quantum critical behavior of the superfluid-Mott glass transition in two space dimensions using large-scale Monte Carlo simulations [31], resolving earlier contradicting predictions in the literature [32–34]. However, magnetic realizations of the Mott glass state have mostly been observed in *three-dimensional* disordered magnets. To the best of our knowledge, quantitative results for the three-dimensional superfluid-Mott glass transition do not yet exist.

To investigate this transition, we analyze a site-diluted three-dimensional quantum rotor model with particle-hole symmetry. We map this quantum Hamiltonian onto a classical $(3+1)$-dimensional XY model with columnar defects. We then carry out Monte Carlo simulations for systems of up to 56 million lattice sites, averaging each data set over 2500–20 000 disorder configurations. For dilutions p below the lattice percolation threshold $p_c \approx 0.688\,392$ [35], we find the superfluid-Mott glass quantum phase transition to be characterized by universal (dilution-independent) critical exponents. The dynamical exponent takes the value $z = 1.67(6)$, and the correlation length exponent is $\nu = 0.90(5)$, fulfilling the inequality $\nu > 2/d$ [36,37]. For the order-parameter exponent β and the susceptibility exponent γ, we find $\beta/\nu = 1.09(3)$ and $\gamma/\nu = 2.50(3)$, respectively. This gives an anomalous dimension of $\eta = -0.50(3)$. These exponents fulfill the hyperscaling relation $2\beta/\nu + \gamma/\nu = d + z$. As a byproduct, our simulations also yield the critical behavior of the clean (undiluted) four-dimensional XY model with high accuracy. It is characterized by mean-field exponents with logarithmic corrections (as expected at the upper critical dimension) and agrees well with the predictions of a generalized scaling theory [38].

Our paper is organized as follows. Section II defines the three-dimensional quantum rotor Hamiltonian and the quantum-to-classical mapping to a $(3+1)$-dimensional classical XY model. It also introduces our finite-size scaling technique (that does not require prior knowledge of the dynamical exponent) as well as the generalized scaling theory [38] for the clean case. Monte Carlo results for the clean and disordered phase transitions are presented in Sec. III. We summarize and conclude in Sec. IV.

II. THEORY

A. Diluted rotor model

We investigate the superfluid-Mott glass transition by means of a site-diluted quantum rotor model residing on a three-dimensional cubic lattice,

$$H = \frac{U}{2}\sum_i \epsilon_i(\hat{n}_i - \bar{n}_i)^2 - J\sum_{\langle ij\rangle}\epsilon_i\epsilon_j\cos(\hat{\phi}_i - \hat{\phi}_j), \quad (1)$$

where $\hat{n}_i$, $\bar{n}_i$, and $\hat{\phi}_i$ are the number operator, offset charge, and phase operator of site i, respectively. U and J represent, respectively, the charging energy and Josephson junction coupling of the sites. We define the dilution, or impurity concentration, as the probability p that a site is vacant. The independent quenched random variables ϵ_i then take on the values 0 (vacancy) with probability p and 1 (occupied site) with probability $1-p$.

The superfluid and Mott glass states can be modeled by this Hamiltonian when considering a particle-hole symmetric system with offset charges $\bar{n}_i = 0$ and commensurate (integer) fillings $\langle\hat{n}_i\rangle$. The phase diagram of this Hamiltonian has been extensively studied [17,22]. For dominant charging energy, $U \gg J$, the ground state is a Mott insulator. For dominant Josephson junction coupling, $J \gg U$, the ground state of the system instead becomes a superfluid. Of course, this behavior is only relevant for dilutions below the lattice percolation threshold, $p_c \approx 0.688\,392$. Dilutions above p_c cause the lattice to break down into disconnected finite-size clusters, preventing the establishment of any long-range ordered superfluid phase. Between the superfluid and Mott insulator phases, a third, intermediate phase emerges. In our particle-hole symmetric case, this is the Mott glass, an incompressible, gapless insulator. The quantum phase transition from the superfluid to the Mott glass state is the focus of the present investigation. A detailed discussion of these phases and their properties can be found, e.g., in Ref. [30].

B. Quantum-to-classical mapping

As we are interested only in universal properties of the transition, we simplify our study of the critical behavior by mapping the 3D quantum Hamiltonian (1) onto a classical Hamiltonian of total dimensionality $D = d + 1 = 4$ [39]. The mapping gives (see Fig. 1)

$$H_{\rm cl} = -J_s\sum_{\langle ij\rangle,\tau}\epsilon_i\epsilon_j\mathbf{S}_{i,\tau}\cdot\mathbf{S}_{j,\tau} - J_\tau\sum_{i,\tau}\epsilon_i\mathbf{S}_{i,\tau}\cdot\mathbf{S}_{i,\tau+1}, \quad (2)$$

with $\mathbf{S}_{i,\tau}$ being an O(2) unit vector at space coordinate i and imaginary-time coordinate τ. Within this mapping, the "classical" temperature T of the Hamiltonian (2) does not refer to the physical temperature of the quantum system (which is zero at the quantum phase transition). Instead, the constants J_s/T and J_τ/T that appear in the classical partition function represent the coupling constants J and U of the quantum system, and the "classical" temperature is used to tune the couplings and drive the system through the transition. Additionally, the expected universality of the critical behavior allows us to ignore the exact numerical values of J_s and J_τ, so we set $J_s = J_\tau = 1$ in the following.

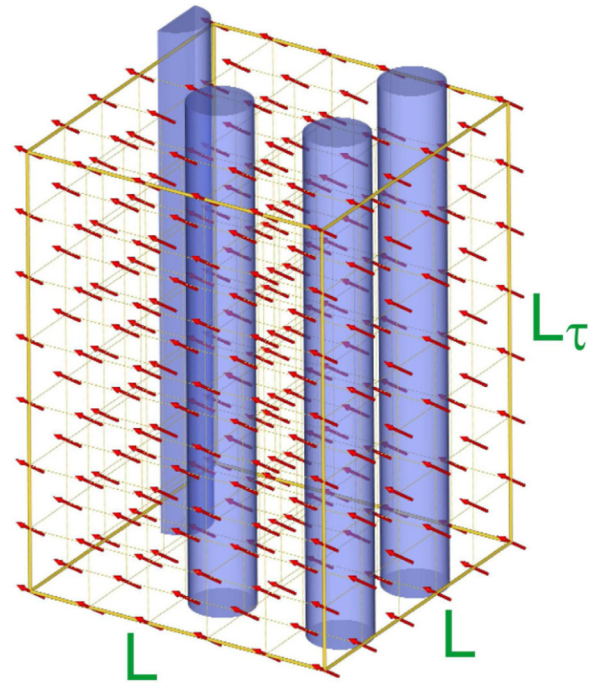

FIG. 1. (2+1)-dimensional analog of the system (2). Arrows are the classical spins $\mathbf{S}$. Columns represent the site vacancies perfectly correlated in imaginary time. A true sketch of the system (2) would be four-dimensional with vacant "columns" in the imaginary-time dimension.

C. Clean (undiluted) critical behavior

In the clean limit $p = 0$ (no vacancies), the Hamiltonian (2) becomes isotropic in the space and imaginary-time dimensions, thus simplifying the system to the four-dimensional classical XY model. This places the clean system at the upper-critical dimension $D_c^+ = 4$ of the XY universality class. Renormalization-group calculations have shown that the transition at D_c^+ exhibits mean-field critical behavior with logarithmic corrections to scaling [38]. These calculations yield a scaling form for the free energy,

$$f_L(r, H) = L^{-4}\mathcal{F}(rL^2(\ln L)^{1/10}, HL^3(\ln L)^{1/4}), \quad (3)$$

where $r = (T - T_c)/T_c$ and H represent the reduced temperature and field conjugate to the order parameter, respectively. Appropriate derivatives of $f_L(r, H)$ yield the dependencies of the order parameter m and its susceptibility χ on the system

size L at criticality,

$$m \propto L^{-1}(\ln L)^{1/4}, \tag{4}$$

$$\chi \propto L^{2}(\ln L)^{1/2}. \tag{5}$$

This implies $\beta/\nu = 1$ and $\gamma/\nu = 2$ for the order parameter and susceptibility critical exponents, respectively. The correlation length exponent can also be extracted via the quantity $d(\ln m)/dT$, which from (3) leads to the scaling form

$$\frac{d(\ln m)}{dT} \propto L^{2}(\ln L)^{1/10} \tag{6}$$

implying a correlation length exponent $\nu = 1/2$. This value, however, violates the Harris criterion [36] for stability of phase transitions against weak disorder, $d\nu > 2$, where $d = 3$ is the number of dimensions with randomness, i.e., the space dimensionality. Thus the clean XY critical point is unstable against the columnar defects we introduce. As a result, we expect the diluted system to exhibit new critical behavior and exponents.

D. Anisotropic finite-size scaling

Variables of scale dimension zero are especially useful in the determination of a system's critical behavior within the framework of finite-size scaling [40]. For example, central to our study is the Binder cumulant

$$g_{av} = \left[1 - \frac{\langle|\mathbf{m}|^4\rangle}{3\langle|\mathbf{m}|^2\rangle^2}\right]_{\rm dis}, \tag{7}$$

where $\mathbf{m} = (1/N)\sum_{i,\tau}\mathbf{S}_{i,\tau}$ is the order parameter [N being the total number of lattice sites of the classical Hamiltonian (2)]. Additionally, $\langle\cdots\rangle$ denotes the Monte Carlo average, and $[\cdots]_{\rm dis}$ is an average over disorder configurations. In the thermodynamic limit, $g_{\rm av}$ is expected to take the value 2/3 in the superfluid phase and the value 1/3 in both the Mott glass and Mott insulator phases. We also study the correlation lengths in the space and imaginary-time directions [41–43]

$$\xi_s = \left[\left(\frac{\tilde{G}(0,0) - \tilde{G}(q_{s0},0)}{q_{s0}^2\tilde{G}(q_{s0},0)}\right)^{1/2}\right]_{\rm dis}, \tag{8}$$

$$\xi_\tau = \left[\left(\frac{\tilde{G}(0,0) - \tilde{G}(0,q_{\tau 0})}{q_{\tau 0}^2\tilde{G}(0,q_{\tau 0})}\right)^{1/2}\right]_{\rm dis} \tag{9}$$

where $\tilde{G}(q_{s0}, q_{\tau 0})$ is the Fourier transform of the spin-spin correlation function, and q_{s0} and $q_{\tau 0}$ are the minimum wavelengths in the space and imaginary-time directions, respectively.

For an isotropic system of system size L and distance $r = (T - T_c)/T_c$ from criticality, the Binder cumulant has the finite-size scaling form $g_{\rm av}(r, L) = X(rL^{1/\nu})$. This guarantees that at $r = 0$, the $g_{\rm av}$ versus r plots for different system sizes will cross at a value $g_{\rm av}(0, L) = X(0)$, allowing us to easily locate T_c. However, the introduction of quenched disorder in the space dimensions breaks the isotropy between space and imaginary time, thus requiring us to distinguish the system sizes L in the space direction and L_τ in the imaginary-time direction.

The finite-size scaling form of the Binder cumulant now depends on the relation between L and L_τ. For conventional power-law scaling, it reads

$$g_{\rm av}(r, L, L_\tau) = X_{g_{\rm av}}(rL^{1/\nu}, L_\tau/L^z), \tag{10}$$

where z is the dynamical exponent, whereas for activated scaling the term L_τ/L^z in (10) is replaced by $\ln(L_\tau)/L^\psi$ with ψ the tunneling exponent. A classification scheme based on the dimensionality of locally ordered rare regions in the disordered system suggests that we should expect power-law scaling [20,44]. Rare region dimensionality for our XY model is $d_{\rm RR} = 1$ (infinitely extended rare regions in the single imaginary-time direction). The lower critical dimension of the XY model is $D_c^- = 2$, thus we have $d_{\rm RR} < D_c^-$. This puts the system (2) firmly into class A of the classification implying power-law dynamical scaling [44]. This also means that our system is not expected to display power-law Griffiths singularities. Instead, observables such as the order-parameter susceptibility χ show conventional behavior. Specifically, χ will remain finite in the Mott glass phase, and rare regions make exponentially small contributions.

For anisotropic systems, we must modify our approach to finite-size scaling. Due to our initial ignorance of the dynamical exponent z, we do not know the appropriate sample sizes $L \times L_\tau$ to fix the second argument of the scaling function (10) in the simulations. We can take advantage of some of the Binder cumulant's properties to find the appropriate ratios ("optimal shapes") of L_τ/L and thus our dynamical exponent z [45–47]. For a fixed spatial size L, $g_{\rm av}$ as a function of L_τ will exhibit a maximum at the point $(L_\tau^{\rm max}, g_{\rm av}^{\rm max})$. At this point, the ratio L_τ/L behaves like the corresponding ratio of correlation lengths ξ_τ/ξ_s and designates the "optimal shape" for that given L. For values of L_τ above or below the maximum, the system can be decomposed into independent blocks which decreases the value of $g_{\rm av}$. At criticality $L_\tau^{\rm max}$ is proportional to L^z. Samples of optimal shape thus fix the second argument of the scaling form (10), allowing one to carry out the rest of the finite-size scaling analysis as usual.

Actually carrying out the calculations requires an iterative approach. An educated guess is made for an initial value of the dynamical exponent z [e.g., the value calculated for the (2+1)D case] [31]. The (approximate) crossings of the $g_{\rm av}$ versus r curves for samples of the resulting shapes give an estimate for T_c. The temperature is then fixed at this estimate of T_c and $g_{\rm av}$ as a function of L_τ is analyzed. The points of maximum value $g_{\rm av}^{\rm max}$ at $L_\tau^{\rm max}$ can then be calculated and give improved estimates for the optimal shapes and thus an improved estimate on z. For $T > T_c$, the $g_{\rm av}^{\rm max}$ values will tend toward their disordered (decreasing) values with increasing system size, while for values $T < T_c$ they tend toward their ordered (increasing) values for increasing system size. Thus, for a given estimate for T_c, the trends of $g_{\rm av}^{\rm max}$ with system size allow us to determine how to adjust our T_c estimate for the next iteration. Using this procedure, the values of T_c and z converge quickly, requiring only about three to five iterations.

Once we have determined the value of z for the system, the usual finite-size analysis can be carried out with the scaling forms

$$m = L^{-\beta/\nu}X_m(rL^{1/\nu}, L_\tau/L^z), \tag{11}$$

$$\chi = L^{\gamma/\nu}X_\chi(rL^{1/\nu}, L_\tau/L^z), \tag{12}$$

where β and γ are the order parameter and susceptibility critical exponents, and the functions X_m and X_χ are scaling functions. Analogously, the reduced correlation lengths ξ_s/L and ξ_τ/L_τ take the scaling forms

$$\xi_s/L = X_{\xi_s}(rL^{1/\nu}, L_\tau/L^z), \tag{13}$$

$$\xi_\tau/L_\tau = X_{\xi_\tau}(rL^{1/\nu}, L_\tau/L^z). \tag{14}$$

We can also establish information about the compressibility κ and superfluid density ρ_s of the system. Under the quantum-to-classical mapping, the compressibility $\kappa = \partial\langle n\rangle/\partial\mu$ and superfluid density ρ_s map, respectively, onto the spin-wave stiffnesses in imaginary-time and space dimensions as

$$\rho_{\mathrm{cl},\tau} = L_\tau^2(\partial^2 f/\partial\theta^2)_{\theta=0}, \tag{15}$$

$$\rho_{\mathrm{cl},s} = L^2(\partial^2 f/\partial\theta^2)_{\theta=0}, \tag{16}$$

where f is the free-energy density for twisted boundary conditions [i.e., the XY spins of the classical model $\mathbf{S}_{i,\tau}$ at $\tau = 0$ $(i = 0)$ are at an angle θ with respect to the spins at the boundary $\tau = L_\tau$ $(i = L)$]. Explicitly, for the XY model considered here (15) takes the form [48]

$$\rho_{\mathrm{cl},\tau} = \frac{1}{N}\sum_{i,\tau}\langle \mathbf{S}_{i,\tau}\cdot\mathbf{S}_{i,\tau+1}\rangle - \frac{\beta}{N}\left\langle\left\{\sum_{i,\tau}\hat{k}\cdot(\mathbf{S}_{i,\tau}\times\mathbf{S}_{i,\tau+1})\right\}^2\right\rangle, \tag{17}$$

where $\hat{k}$ represents the unit vector perpendicular to the XY plane of the spins. The space stiffness $\rho_{\mathrm{cl},s}$ takes an analogous form. These quantities are expected to exhibit power-law scaling behavior according to the scaling forms

$$\rho_{\mathrm{cl},s} = L^{-y_s}X_{\rho_s}(rL^{1/\nu}, L_\tau/L^z), \tag{18}$$

$$\rho_{\mathrm{cl},\tau} = L^{-y_\tau}X_{\rho_\tau}(rL^{1/\nu}, L_\tau/L^z), \tag{19}$$

where X_{ρ_s} and X_{ρ_τ} are scaling functions, while $y_s = d + z - 2$ and $y_\tau = d - z$ are the scale dimensions of the spin-wave stiffnesses in space and imaginary time, respectively [30]. Both stiffnesses are expected to be nonzero in the superfluid phase. In both the Mott insulator and the Mott glass phases, they are expected to vanish. (Note that the Mott glass is an *incompressible* insulator.)

III. MONTE CARLO SIMULATIONS

A. Overview

Our investigation consists of Monte Carlo simulations of the classical XY model (2) with both the standard single-spin-flip METROPOLIS [49] algorithm as well as the cluster-update Wolff [50] algorithm. Both algorithms are used throughout the simulations, and one "full sweep" is defined as a METROPOLIS sweep over the entire lattice and a Wolff sweep. A Wolff sweep in our simulations flips a number of clusters such that the total number of spins flipped in the clusters is equal to the number of spins in the system. While the Wolff algorithm alone is sufficient to equilibrate clean systems, highly dilute systems can exhibit small disconnected clusters that the METROPOLIS algorithm can more effectively equilibrate.

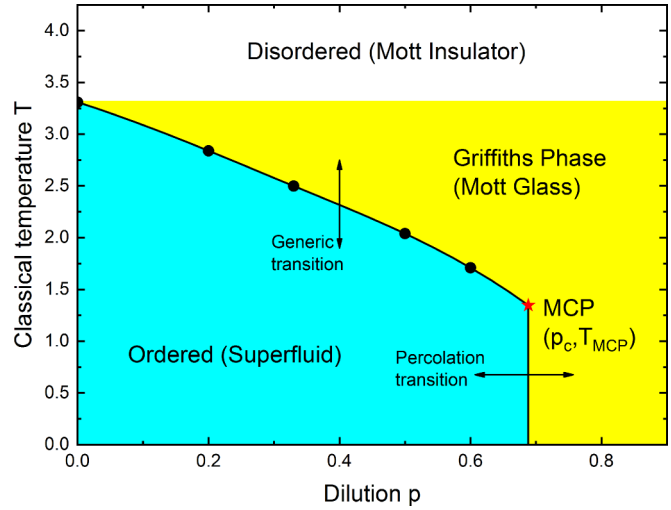

FIG. 2. Phase diagram of the classical (3+1)-dimensional XY model with respect to classical temperature T and dilution p. The multicritical point (MCP) is estimated as the intersection of a spline interpolation of the numerical critical temperatures (dots) and the percolation transition at p_c. The errors of the calculated T_c are smaller than the symbol size.

We simulate a range of dilutions $p = 0, 1/3, 1/2, 3/5$ and $p = p_c \approx 0.688\,392$ with system sizes up to $L = 80$ in the space dimensions and $L_\tau = 320$ in the imaginary-time dimension. All data need to be averaged over a large number of independent dilution configurations. This increases the computational effort needed for meaningful results. Best performance can be achieved with a rather small number of measurements sweeps, N_m, but a large number of disorder realizations (samples), N_s [51,52]. To this end, we have chosen $N_m = 500$ and $N_s = 4000$–$20\,000$ (depending on system size). To eliminate biases due to the short measurements, we use improved estimators [53]. To ensure complete equilibration of the system, we have chosen $N_{\mathrm{eq}} = 100$ equilibration sweeps to be carried out before each measurement. We have confirmed that 100 sweeps are sufficient by comparing the results of the simulations with hot starts (spins initially randomly oriented) and cold starts (spins initially aligned) and verifying that they agree within their error bars.

The phase diagram resulting from the simulations is presented in Fig. 2. As expected, the transition temperatures $T_c(p)$ decrease with increasing dilution from the clean value $T_c(0)$. The generic transition ends at the multicritical point, which we have estimated from the intersection of a spline fit of the calculated $T_c(p)$ and the lattice percolation threshold $p_c = 0.688\,392$.

B. Clean critical behavior

First, we analyze the phase transition of the clean, undiluted system $(p = 0)$. Since the clean system is isotropic, we choose samples with $L = L_\tau$ between 10 and 80. The critical temperature is determined from the crossings of the g_{av} versus T curves for different L and the corresponding crossings of

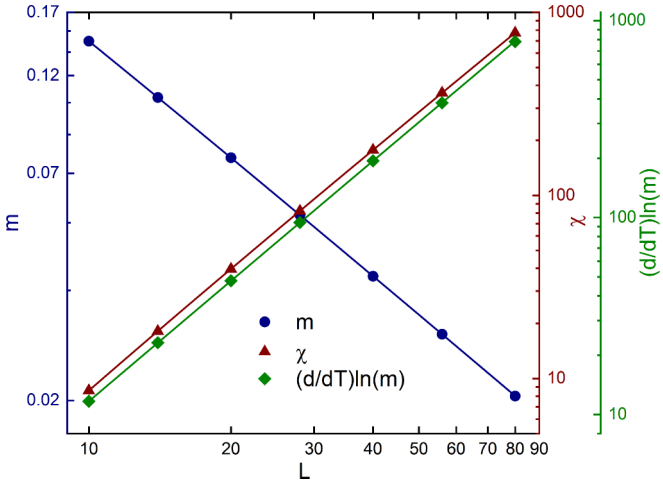

FIG. 3. Order parameter m and susceptibility χ vs system size L for the clean case ($p = 0$). Solid lines are fits to $m = aL^{-\beta/\nu}[\ln(L/L_0)]^{\omega}$ and $\chi = aL^{\gamma/\nu}[\ln(L/L_0)]^{\omega}$ that yield $\beta/\nu = 1.008(12)$ and $\gamma/\nu = 2.00(1)$, respectively. Statistical errors are of the order of the symbol size.

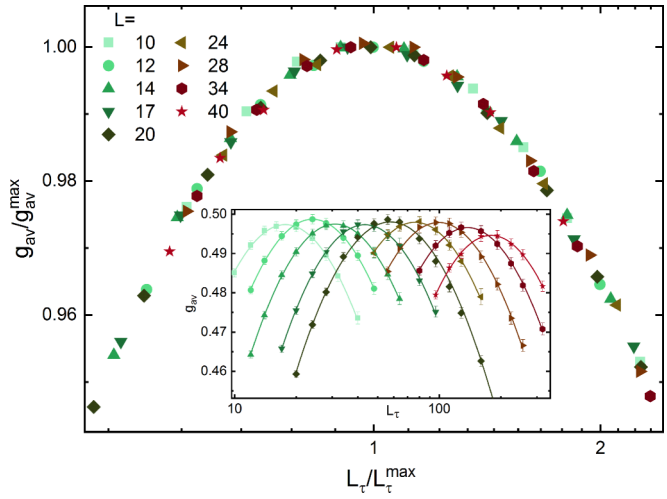

FIG. 4. Binder cumulant $g_{\rm av}$ as a function of L_τ for several L and dilution $p = 0.5$ at the critical temperature $T_c = 2.037$. Plotting $g_{\rm av}/g_{\rm av}^{\rm max}$ in the main panel eliminates the leading additive correction to scaling from the analysis.

the ξ/L versus T curves. Extrapolating to $L \to \infty$ yields a critical temperature $T_c(0) = 3.314\,45(3)$.

Figure 3 shows both order parameter and susceptibility as functions of system size right at the critical temperature. Fits of the order-parameter data to the scaling form $m = aL^{-\beta/\nu}[\ln(L/L_0)]^{\omega}$ are of good quality (reduced chi-squared $\tilde{\chi}^2 \approx 0.3$) and give critical exponents $\beta/\nu = 1.008(12)$ and $\omega = 0.25(8)$. Considering the same fits for various temperatures within the error bars of our critical temperature estimate leads to variation in β/ν of around 0.02. Our final estimate for the order-parameter exponent is $\beta/\nu = 1.00(2)$.

Fits of the susceptibility to the scaling form $\chi = aL^{\gamma/\nu}[\ln(L/L_0)]^{\omega'}$ are less stable. We fit the data to the scaling form with the irrelevant exponent fixed at its predicted value $\omega' = 1/2$ from Eq. (5). This yields a critical exponent $\gamma/\nu = 2.00(2)$ with reduced chi-squared $\tilde{\chi}^2 \approx 0.65$. Susceptibility fits are more sensitive to errors in critical temperature, having a variation in γ/ν of about 0.04 for temperatures within our error bar estimates. Our final estimate for the susceptibility critical exponent is $\gamma/\nu = 2.00(6)$.

Lastly, we find the correlation length critical exponent via slopes of the Binder cumulant $g_{\rm av}$, reduced correlation length ξ/L, and logarithm of the order parameter $\ln(m)$, with respect to temperature. Equation (6) predicts a value of $\nu = 1/2$ for the correlation length critical exponent for $(d/dT)\ln(m)$, and universality implies the same scaling form holds for $g_{\rm av}$ and ξ/L. Fitting the data for $(d/dT)\ln(m)$ to the scaling form $aL^{1/\nu}\ln(L/L_0)^{\bar{\omega}}$ with the irrelevant exponent fixed at the theoretical value $\bar{\omega} = 1/10$ yields the critical exponent $\nu = 0.50(2)$ for an acceptable fit ($\tilde{\chi}^2 \approx 4$). Similar analysis for $(d/dT)g_{\rm av}$ and $(d/dT)(\xi/L)$ yields $\nu = 0.50(2)$ and $\nu = 0.49(4)$, respectively. Our final estimate for the correlation length critical exponent is $\nu = 0.50(6)$.

Finally, we note that pure power-law fits to the data show significantly larger $\tilde{\chi}^2$ values. This further justifies the logarithmic corrections in the scaling forms (4)–(6). In summary, all of our Monte Carlo results for the clean case are in good agreement with the scaling theory of Ref. [38].

C. Disordered case: Generic transition

The finite-size scaling analysis of the generic transition ($0 < p < p_c$) is carried out as described in Sec. II D. Determining a full set of critical exponents requires first finding the optimal shapes and calculating the dynamical exponent z in order to fix the second argument of our scaling forms (10)–(19). This is achieved using the iterative procedure also outlined in Sec. II D.

Figures 4 and 5 show an example of this analysis. Specifically, Fig. 4 presents the Binder cumulant $g_{\rm av}$ for the dilution $p = 0.5$ as a function of L_τ for system sizes $L = 10$–40 at the estimated critical temperature. The raw data are shown in the inset; as expected, $g_{\rm av}^{\rm max}$ at the critical point is (roughly)

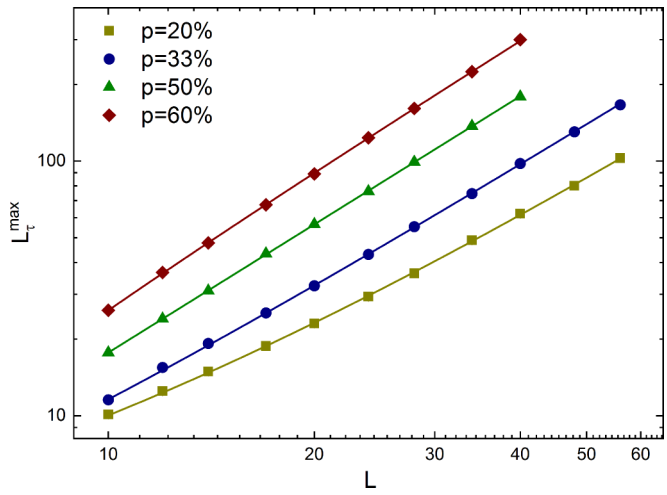

FIG. 5. Log-log plots of $L_\tau^{\rm max}$ vs L. Solid lines are fits to $L_\tau^{\rm max} = aL^z(1 + bL^{-\omega})$ yielding $z = 1.672(9)$ and $\omega = 1.18(5)$. Statistical errors are of the order of the symbol size.

independent of L and exhibits a maximum at $L_\tau^{\max}$ for each system size. The remaining variation of $g_{\rm av}^{\max}$ is due to the uncertainty in T_c for the large system sizes and corrections to scaling for small system sizes (both of these will be discussed further below). The main panel is a scaling plot demonstrating that the Binder cumulant fulfills the scaling form (10) to a high degree of accuracy, and variations due to uncertainty in T_c and corrections to scaling simply shift the $g_{\rm av}$ versus L_τ curves up or down. Corresponding scaling plots were also constructed with analogous results for the remaining dilutions $p = 1/5$, $1/3$, and $3/5$.

Determining z requires analyzing the position $L_\tau^{\max}$ of these maxima, which we have found via quadratic fits of $g_{\rm av}$ versus $\ln L_\tau$. Plots of $L_\tau^{\max}$ versus L are shown in Fig. 5. As can be seen, the data show significant corrections to scaling (deviations from straight lines), especially for smaller dilutions. Neglecting them by fitting the data via pure power laws would yield only effective, scale-dependent exponents. Therefore, we include the leading-order correction to scaling via the ansatz $L_\tau^{\max} = aL^z(1 + bL^{-\omega})$ with dilution-independent critical exponents z and ω but dilution-dependent prefactors a and b. This yields true asymptotic, scale-independent critical exponents. Combined fits of all four dilution data sets gives exponents $z = 1.672(9)$ and $\omega = 1.18(5)$ with an acceptable reduced chi-squared $\tilde{\chi}^2 \approx 2.69$. If we consider the robustness of the combined fits against removal of upper and lower data points from each set as well as removal of entire dilution sets, we come to an estimate for the dynamical critical exponent of $z = 1.67(4)$. We also note that the leading corrections to scaling vanish close to $p = 1/2$ where the prefactor b changes sign and is effectively zero for our fits of $p = 1/2$. The vanishing of these corrections is also reinforced by the comparison of pure power-law fits and fits to scaling forms including subleading corrections. For $p = 1/2$, power-law fits yield $z = 1.671(3)$, where the fits including the subleading corrections yield $z = 1.66(1)$. The global, dilution-independent value for the dynamical exponent is also bracketed nicely by the values obtained upon pure power-law fits of the largest system sizes for the dilutions $p = 1/3$ and $3/5$, which yield $z = 1.592(6)$ and $1.767(7)$, respectively. To estimate the error of z stemming from the uncertainty in T_c, we have repeated the analysis for appropriately chosen temperatures slightly above and below our estimate for T_c. Variation of the dynamical exponent within this range of temperatures is about 0.03. After considering this uncertainty in T_c, the statistical error, and the robustness of our fits, we come to our final estimate of the dynamical exponent $z = 1.67(6)$.

To complete our set of critical exponents, we now analyze the Monte Carlo runs for systems of optimal shape and in the vicinity of their critical temperature $T_c(p)$. With L_τ/L^z fixed by the optimal shapes found above, the scaling forms (11) and (12) are then used to extract β/ν and γ/ν from the L dependence of the order parameter m and susceptibility χ at $T_c(p)$. We again fit the data with leading corrections to scaling included via the ansatz $m = aL^{-\beta/\nu}(1 + bL^{-\omega})$ and $\chi = aL^{\gamma/\nu}(1 + bL^{-\omega})$ with universal exponents but dilution-dependent prefactors. However, the combined fits of these data proved to be very sensitive to small changes in $T_c(p)$ (much more so than the fit determining z). This indicates that our critical temperature estimates (originally found from the crossings of the curves of dimensionless quantities versus temperature) are not the true critical temperatures. Thus, to improve our critical temperature estimates, we impart the criterion that at criticality the value of $g_{\rm av}^{\max}$ should approach a dilution-independent value as $L \to \infty$. We can adjust our estimates for $T_c(p)$ until this criterion is satisfied, with $g_{\rm av}^{\max}$ approaching dilution and system-size-independent values, as is shown in Fig. 6 [31]. This adjustment of the critical temperatures yields our final estimates: $T_c(1/5) = 2.837$, $T_c(1/3) = 2.4973$, $T_c(1/2) = 2.0332$, $T_c(3/5) = 1.7103$. The data can also be seen to satisfy this criterion for a small range of temperatures, thus we assign an error to our estimated critical temperatures of no more than ± 0.0003. The data in Fig. 6 clearly demonstrate that the systems with dilutions $p = 1/3$ and $1/2$ show pronounced corrections to scaling. They are still crossing over from the clean critical fixed point to the asymptotic regime even at the largest L. Moreover, $g_{\rm av}^{\max}$ for small system sizes exhibits nonmonotonous behavior, from which we conclude that there are at least two corrections to scaling contributing for the smallest dilutions and system sizes.

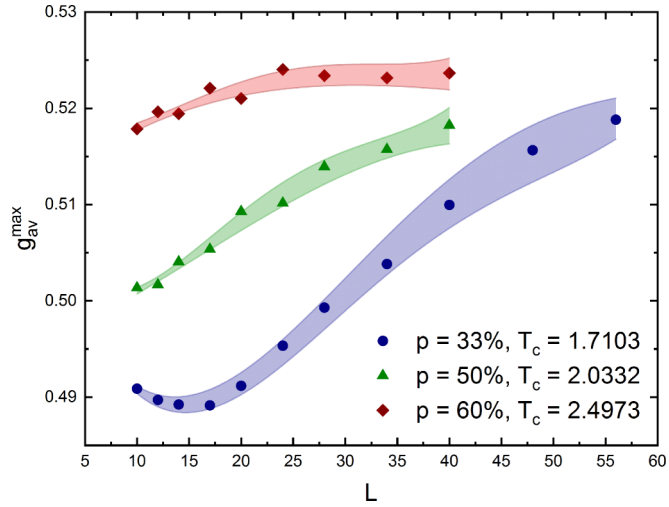

FIG. 6. $g_{\rm av}^{\max}$ vs L for the improved estimates for T_c. Shaded regions represent the range values for which the criterion is also satisfied. From this we estimate an error on T_c of no more than 0.0003. Statistical errors are of the order of the symbol size or smaller. The remaining variation of $g_{\rm av}^{\max}$ likely stems from the discreteness of L_τ.

With the improved estimates for T_c, we proceed to fit the three largest dilutions ($p = 1/5, 1/3, 3/5$) with the above scaling ansatz to find β/ν and γ/ν. Order parameter m versus system size L for the three dilutions is shown in Fig. 7. We perform a combined fit with $m = aL^{-\beta/\nu}(1 + bL^{-\omega})$. Leaving out the system sizes most affected by the second subleading corrections to scaling mentioned above, we get good fits ($\tilde{\chi}^2 \approx 0.43$) that result in a critical exponent $\beta/\nu = 1.087(11)$ and correction exponent $\omega = 1.22(7)$. Fits to the same data for slightly adjusted temperatures within the estimated error ($T_c \pm 0.0003$) lead to variation in the critical exponent of about 0.02. Our final estimate for the order parameter critical exponent then reads $\beta/\nu = 1.09(3)$.

Figure 8 shows the order-parameter susceptibility χ as a function of system size L at criticality. Fitting to the ansatz with leading-order corrections $\chi = aL^{\gamma/\nu}(1 + bL^{-\omega})$, and again

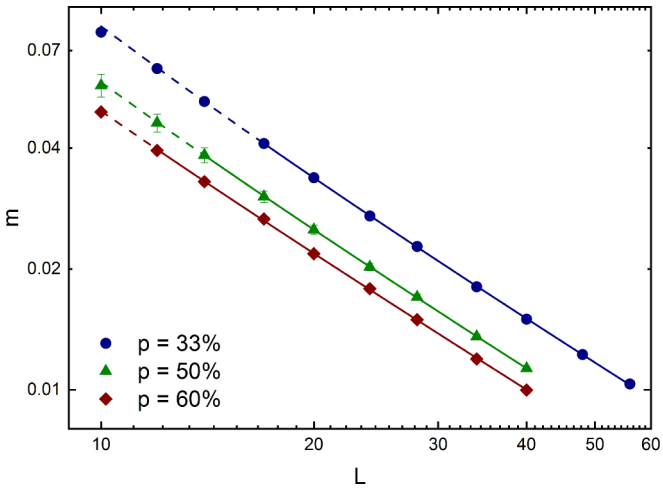

FIG. 7. Log-log plot of m vs L at the critical temperature. Solid lines are fits to $m = aL^{-\beta/\nu}(1 + bL^{-\omega})$ that yield $\beta/\nu = 1.087(11)$ and $\omega = 1.22(7)$. Lines are dashed in regions that are not included in the fit. Statistical errors are of the order of the symbol size unless shown explicitly in the plot.

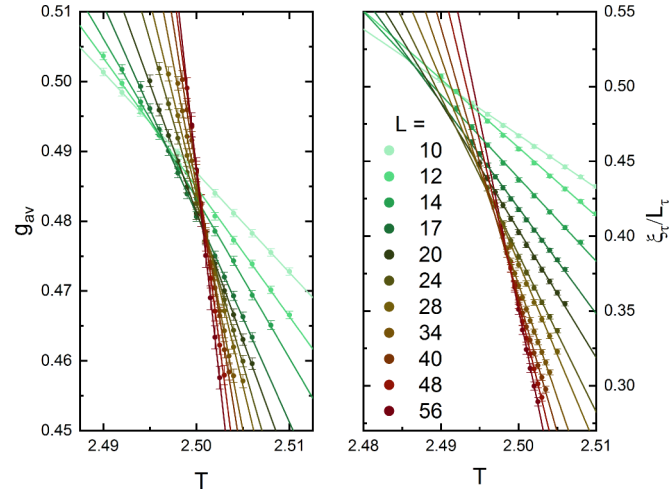

FIG. 9. Binder cumulant $g_{\rm av}$ and reduced correlation function ξ_τ/L_τ for systems of optimal shape and dilution $p = 1/3$. Plotted are system sizes $L = 10$–56 with increasing slope.

dropping the system sizes most affected by subleading order corrections, we arrive at a good fit ($\tilde{\chi}^2 \approx 1.3$) that yields the critical exponent $\gamma/\nu = 2.495(7)$ and correction exponent $\omega = 1.16(2)$. After considering the uncertainties in T_c and the fit range, as we did for β/ν, we come to the final estimate for the susceptibility exponent $\gamma/\nu = 2.50(3)$.

We now move to determining the correlation length critical exponent. This can be determined by considering the slopes of $g_{\rm av}$ and ξ_τ/L_τ as functions of temperature. Figure 9 shows off-critical data $g_{\rm av}$ and ξ_τ/L_τ for dilution $p = 1/3$, as functions of temperature. Since both quantities have scale dimension zero, they should cross directly at the critical temperature. However, it is clear in the data that a shift occurs in these crossings for increasing system size L, thus we still expect significant corrections to scaling. Equations (10) and (13) show that the correlation exponent can be extracted from finite-size scaling of $(d/dT)g_{\rm av}$ and $(d/dT)\xi_\tau/L_\tau$, each of which varies as $L^{1/\nu}$ with system size. Extracting the slopes of each of these functions is done by linear fits to the data in the vicinity of the critical temperature. Figure 10 shows the slopes of the Binder cumulant $g_{\rm av}$ as a function of system size. Again, to account for the corrections to scaling, we fit these data with the ansatz scaling form $aL^{1/\nu}(1 + bL^{-\omega})$. Combined fits to $(d/dT)g_{\rm av}$ lead to $\nu = 0.90(2)$ and $\omega = 1.17(8)$ with a reduced chi-squared $\tilde{\chi} \approx 2.2$. Similar fits of the reduced correlation length ξ_τ/L_τ are of good quality ($\tilde{\chi}^2 \approx 1.15$) when the smallest system sizes are left out, giving a correlation exponent of $\nu = 0.894(4)$ and a correction exponent $\omega = 1.16(10)$. Similar analysis carried out on $(d/dT)\xi_s/L$ yields nearly identical results. Considering the robustness of the fits against removal

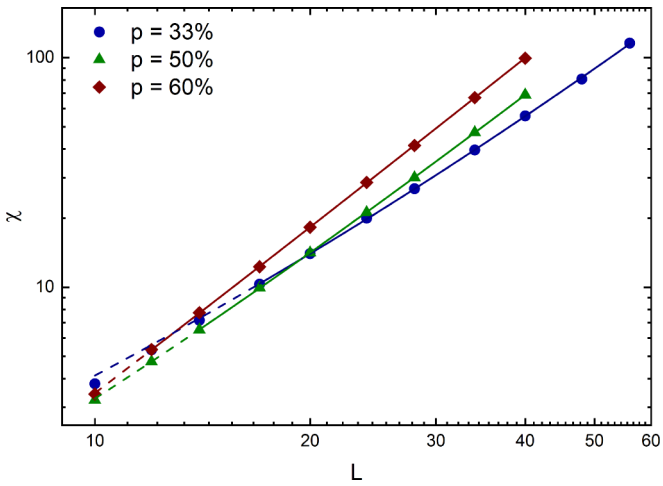

FIG. 8. Log-log plot of χ vs L at the critical temperature. Solid lines are fits to $\chi = aL^{\gamma/\nu}(1 + bL^{-\omega})$ that yield $\gamma/\nu = 2.495(7)$ and $\omega = 1.16(2)$. Lines are dashed in regions that are not included in the fit. Statistical errors are of the order of the symbol size.

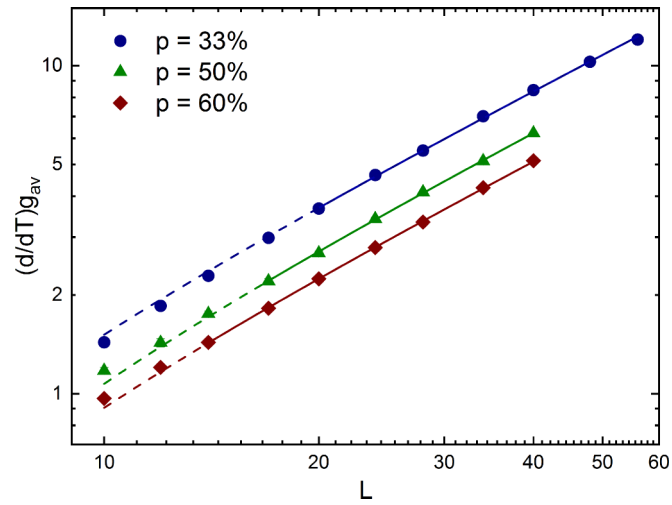

FIG. 10. Log-log plot of $(d/dT)g_{\rm av}$ vs L. Solid lines are fits to $g_{\rm av} = aL^{1/\nu}(1 + bL^{-\omega})$ that yield $\nu = 0.90(2)$ and $\omega = 1.17(8)$. Lines are dashed in regions that are not included in the fit. Statistical errors are of order of the symbol size.

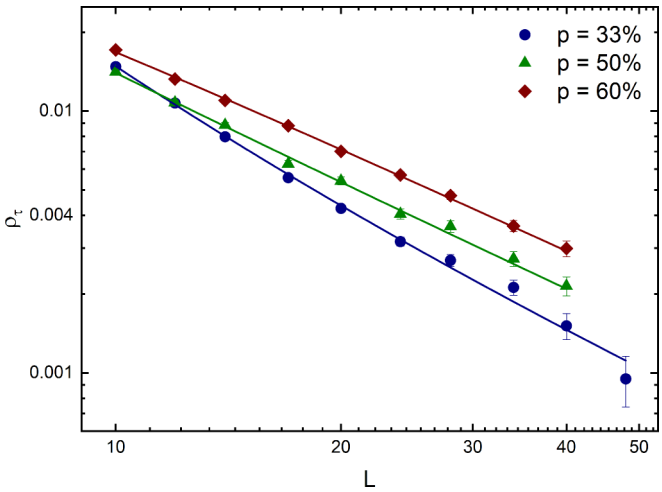

FIG. 11. Log-log plot of ρ_τ vs L. Solid lines are fits to $\rho_\tau = aL^{-y_\tau}(1 + bL^{-\omega})$ that yield $y_\tau = 1.32(2)$ and $\omega = 1.19(6)$.

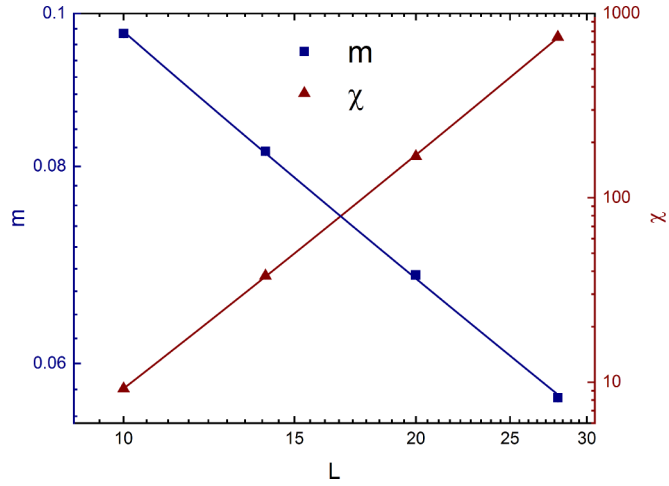

FIG. 12. Log-log plot of observables m and χ for the percolation transition at $p_c = 0.688\,392$ and $T = 1.0$. Dashed lines are fits to the expectations [54]. Statistical errors are of the order of the symbol size.

of upper and lower data points, we are led to a somewhat larger error, leading to a final estimate that reads $\nu = 0.90(5)$.

The critical exponents must satisfy the hyperscaling relationship $2\beta/\nu + \gamma/\nu = d + z$, where $d = 3$ is the spatial dimension. Our values $\beta/\nu = 1.09(3)$, $\gamma/\nu = 2.50(3)$, and $z = 1.67(6)$ fulfill this relationship nicely within the error bars. We can also assign a value to the anomalous dimension η, defined via the decay of the critical correlation function in space, $G(\mathbf{x}) \sim |\mathbf{x}|^{-(d+z-2+\eta)}$. It measures the deviation of G from a hypothetical Gaussian theory.[1] This anomalous dimension η can be calculated via the relationship $\eta = 2 - \gamma/\nu$, giving the result $\eta = -0.50(3)$. Additionally, the inequality $d\nu > 2$ is now fulfilled for our correlation exponent $\nu = 0.90(5)$. Because the critical exponents satisfy the hyperscaling relationship and the values of the exponent ω that governs the corrections to scaling are consistent across the range of fits, we can conclude that the critical exponent estimates that we have obtained are the true asymptotic critical exponents.

D. Superfluid density

A final result from our simulations is the critical behavior of the compressibility κ and superfluid density ρ_s. This is determined by considering the behavior of the spin-wave stiffness of the classical Hamiltonian (2) in space and imaginary-time dimensions for optimally shaped systems right at the critical temperatures for the dilutions $p = 1/3, 1/2, 3/5$. Both observables, $\rho_{\mathrm{cl},s}$ and $\rho_{\mathrm{cl},\tau}$, are very close to zero and thus noisy. A plot of $\rho_{\mathrm{cl},\tau}$ versus L is shown in Fig. 11. Corrections to scaling are clearly still relevant, so we perform fits with first-order corrections $\rho_{\mathrm{cl},\tau} = aL^{-y_\tau}(1 + bL^{-\omega})$. Good fits can be obtained over the entire data set despite the noisy large system sizes ($\tilde{\chi}^2 \approx 1.03$), yielding $y_\tau = 1.32(1)$ and $\omega = 1.19(6)$. The fit is surprisingly stable against removal of data points and dilution sets. We quote our final estimate of this exponent as $y_\tau = 1.32(2)$. This satisfies the generalized Josephson relation [17] for the compressibility $y_\tau = d - z$ within error bars.

Spin-wave stiffness in the space dimensions is much smaller and thus has larger statistical errors. Independent fits were not possible for this data set. However, we fit the data with the functional form $y_s = aL^{-y_s}(1 + bL^{-\omega})$ fixing the exponents via the generalized Josephson relations $y_s = d + z - 2$. Fixing $y_s = 2.67$ and $\omega = 1.18$ (from earlier fits) yields a reasonable fit to the data ($\tilde{\chi}^2 \approx 0.03$), in agreement with expectations.

E. Percolation transition

So far, we have analyzed "generic" transitions that are driven by tuning of the (classical) temperature for dilutions $p < p_c$. Another type of transition—the percolation transition—can occur by tuning the dilution concentration p through the percolation threshold p_c of the lattice at very low temperature. The critical behavior of these transitions is entirely dependent on the critical geometry of percolating lattice with the dynamics of the rotor model unaffected, remaining locally ordered on each percolating cluster. A theory has been developed [54] that predicts the critical behavior of this percolation quantum phase transition. These predictions give exponents $\beta = 0.417$, $\gamma = 4.02$, $\nu = 0.875$, and $z = 2.53$. Note that the static exponents β and ν as well as the percolation threshold p_c agree with the corresponding 3D classical percolation values (see, e.g., Refs. [55–57]).

To test these predictions, we perform simulations with dilution right at the percolation threshold $p = p_c = 0.688\,392$ and temperature $T = 1.0$, well below the estimated multicritical temperature $T_{\mathrm{MCP}} \approx 1.35$. The large value of the predicted z leads to the need for very large system sizes L_τ to confirm the dynamical critical exponent. To reduce the numerical effort, we simulated systems with the dynamical exponent fixed at its predicted value $z = 2.53$ and used these optimally shaped systems to confirm the remaining critical exponents. Figure 12 shows both order

[1] A purely Gaussian theory would predict a correlation function that decays as $G \sim |\mathbf{x}|^{-(d+z)+2}$ with z the dynamical exponent of the system. The anomalous dimension is the deviation of the exponent from this power-law behavior.

parameter m and susceptibility χ for these systems up to $L = 28$. Considering the small system sizes in our data, we fit both sets to their predicted scaling forms with first-order corrections included. For the order-parameter exponent, theory predicts $\beta/\nu \approx 0.476\,57$. Fitting the data to the form $m = aL^{-\beta/\nu}(1 + bL^{-\omega})$ with the critical exponent β/ν fixed at the predicted value leads to a good fit ($\tilde{\chi}^2 \approx 1.41$) with irrelevant exponent $\omega = 0.99(12)$. Similarly, for the susceptibility exponent, theory predicts $\gamma/\nu \approx 4.59429$. Fitting these data to $\chi = aL^{\gamma/\nu}(1 + bL^{-\omega})$ while fixing the critical exponent γ/ν to its predicted value leads to fits of lesser quality ($\tilde{\chi}^2 \approx 5.31$), but still within reasonable agreement with the theory, and giving an irrelevant exponent $\omega = 1.26(58)$.

IV. CONCLUSIONS

In conclusion, we have carried out large-scale Monte Carlo simulations to determine the critical behavior of the superfluid-Mott glass quantum phase transition in three space dimensions. To do so, we have mapped a site-diluted quantum rotor model with commensurate filling and off-diagonal disorder onto a (3+1)-dimensional classical XY model, and simulated it via the standard METROPOLIS and Wolff algorithms.

In the absence of disorder, the superfluid-Mott insulator transition falls into the four-dimensional XY universality class, which features mean-field critical behavior with logarithmic corrections. The correlation exponent takes the value $\nu = 1/2$ that violates the Harris criterion $d\nu > 2$. As a consequence, the superfluid-Mott glass transition occurring in the disordered case shows critical behavior differing from that of the clean case.

This superfluid-Mott glass transition exhibits a conventional finite-disorder quantum critical point with power-law dynamical scaling $\xi_\tau \sim \xi_s^z$ between the correlation time and length. This agrees with a general classification of disordered quantum phase transitions based on rare region dimensionality in the system [20,54]. For the classical (mapped) Hamiltonian (2), the rare regions are infinitely long rods in the time dimension, giving a rare region dimensionality $d_{\mathrm{RR}} = 1$. Comparing this to the lower critical dimension of the classical XY model $D_c^- = 2$, we can see that $d_{\mathrm{RR}} < D_c^-$, putting the system into class A (of conventional power-law scaling), as designated by the classification scheme.

TABLE I. Critical exponents found in this work. Italic values are not calculated directly but represent theoretical values that we have used and/or confirmed in the simulations.

Our results	z	β/ν	γ/ν	ν	η
Clean	*1*	1.00(2)	2.00(6)	0.50(5)	0.00(5)
Diluted	1.67(6)	1.09(3)	2.50(3)	0.90(5)	− 0.50(3)
Percolation	*2.53*	*0.477*	*4.594*	*0.875*	*− 2.594*

For the generic transition occurring for dilutions p below the lattice percolation threshold p_c, we find universal, dilution-independent critical exponents from our Monte Carlo data. These exponents, summarized in Table I, satisfy the hyperscaling relation as well as the Harris criterion. We have also considered the percolation transition that occurs across the percolation threshold p_c at low temperature. The critical behavior of this transition is also of conventional power-law type, and our Monte Carlo data can be fitted well with theoretical behavior predicted within the scaling theory by Vojta and Schmalian [54].

An experimental realization of the three-dimensional superfluid-Mott glass transition can be found in diluted anisotropic spin-1 antiferromagnets. These systems are typically three-dimensional and exhibit particle-hole symmetry naturally as a consequence of the up-down symmetry of the Hamiltonian in the absence of an external magnetic field. Such a realization was recently observed in bromine-doped dichloro-tetakic-thiourea-nickel [12].

Further experimental studies can be carried out in disordered bosonic systems such as ultracold atoms in optical lattices as well as granular superconductors. However, often only *statistical* particle-hole symmetry can be achieved in these systems. Whether or not this statistical particle-hole symmetry will destabilize the Mott glass into a Bose glass remains unresolved.

ACKNOWLEDGMENTS

This work was supported in part by the NSF under Grants No. PHY-1125915 and No. DMR-1506152. T.V. acknowledges the hospitality of the Kavli Institute for Theoretical Physics, where part of the work was performed.

[1] B. C. Crooker, B. Hebral, E. N. Smith, Y. Takano, and J. D. Reppy, Phys. Rev. Lett. **51**, 666 (1983).
[2] J. D. Reppy, Physica B+C **126**, 335 (1984).
[3] D. B. Haviland, Y. Liu, and A. M. Goldman, Phys. Rev. Lett. **62**, 2180 (1989).
[4] A. F. Hebard and M. A. Paalanen, Phys. Rev. Lett. **65**, 927 (1990).
[5] H. S. J. van der Zant, F. C. Fritschy, W. J. Elion, L. J. Geerligs, and J. E. Mooij, Phys. Rev. Lett. **69**, 2971 (1992).
[6] H. S. J. van der Zant, W. J. Elion, L. J. Geerligs, and J. E. Mooij, Phys. Rev. B **54**, 10081 (1996).
[7] M. White, M. Pasienski, D. McKay, S. Q. Zhou, D. Ceperley, and B. DeMarco, Phys. Rev. Lett. **102**, 055301 (2009).
[8] S. Krinner, D. Stadler, J. Meineke, J.-P. Brantut, and T. Esslinger, Phys. Rev. Lett. **110**, 100601 (2013).
[9] C. D'Errico, E. Lucioni, L. Tanzi, L. Gori, G. Roux, I. P. McCulloch, T. Giamarchi, M. Inguscio, and G. Modugno, Phys. Rev. Lett. **113**, 095301 (2014).
[10] A. Oosawa and H. Tanaka, Phys. Rev. B **65**, 184437 (2002).
[11] T. Hong, A. Zheludev, H. Manaka, and L.-P. Regnault, Phys. Rev. B **81**, 060410 (2010).
[12] R. Yu, L. Yin, N. S. Sullivan, J. S. Xia, C. Huan, A. Paduan-Filho, N. F. Oliveira, Jr., S. Haas, A. Steppke, C. F. Miclea, F. Weickert, R. Movshovich, E.-D. Mun, B. L. Scott, V. S. Zapf, and T. Roscilde, Nature (London) **489**, 379 (2012).

[13] D. Hüvonen, S. Zhao, M. Månsson, T. Yankova, E. Ressouche, C. Niedermayer, M. Laver, S. N. Gvasaliya, and A. Zheludev, Phys. Rev. B **85**, 100410 (2012).
[14] A. Zheludev and T. Roscilde, C. R. Phys. **14**, 740 (2013).
[15] T. Giamarchi and H. J. Schulz, Phys. Rev. B **37**, 325 (1988).
[16] D. S. Fisher and M. P. A. Fisher, Phys. Rev. Lett. **61**, 1847 (1988).
[17] M. P. A. Fisher, P. B. Weichman, G. Grinstein, and D. S. Fisher, Phys. Rev. B **40**, 546 (1989).
[18] R. B. Griffiths, Phys. Rev. Lett. **23**, 17 (1969).
[19] M. Thill and D. A. Huse, Physica A **214**, 321 (1995).
[20] T. Vojta, J. Phys. A **39**, R143 (2006).
[21] T. Vojta, J. Low Temp. Phys. **161**, 299 (2010).
[22] P. B. Weichman and R. Mukhopadhyay, Phys. Rev. Lett. **98**, 245701 (2007).
[23] A. Priyadarshee, S. Chandrasekharan, J.-W. Lee, and H. U. Baranger, Phys. Rev. Lett. **97**, 115703 (2006).
[24] H. Meier and M. Wallin, Phys. Rev. Lett. **108**, 055701 (2012).
[25] R. Ng and E. S. Sørensen, Phys. Rev. Lett. **114**, 255701 (2015).
[26] J. P. Álvarez Zúñiga, D. J. Luitz, G. Lemarié, and N. Laflorencie, Phys. Rev. Lett. **114**, 155301 (2015).
[27] Z. Yao, K. P. C. da Costa, M. Kiselev, and N. Prokof'ev, Phys. Rev. Lett. **112**, 225301 (2014).
[28] R. Yu, C. F. Miclea, F. Weickert, R. Movshovich, A. Paduan-Filho, V. S. Zapf, and T. Roscilde, Phys. Rev. B **86**, 134421 (2012).
[29] T. Giamarchi, P. L. Doussal, and E. Orignac, Phys. Rev. B **64**, 245119 (2001).
[30] P. B. Weichman and R. Mukhopadhyay, Phys. Rev. B **77**, 214516 (2008).
[31] T. Vojta, J. Crewse, M. Puschmann, D. Arovas, and Y. Kiselev, Phys. Rev. B **94**, 134501 (2016).
[32] N. Prokof'ev and B. Svistunov, Phys. Rev. Lett. **92**, 015703 (2004).
[33] S. Iyer, D. Pekker, and G. Refael, Phys. Rev. B **85**, 094202 (2012).
[34] M. Swanson, Y. L. Loh, M. Randeria, and N. Trivedi, Phys. Rev. X **4**, 021007 (2014).
[35] H. G. Ballesteros, L. A. Fernández, V. Martín-Mayor, A. M. Sudupe, G. Parisi, and J. J. Ruiz-Lorenzo, J. Phys. A **32**, 1 (1999).
[36] A. B. Harris, J. Phys. C **7**, 1671 (1974).
[37] J. T. Chayes, L. Chayes, D. S. Fisher, and T. Spencer, Phys. Rev. Lett. **57**, 2999 (1986).
[38] R. Kenna, Nucl. Phys. B **691**, 292 (2004).
[39] M. Wallin, E. S. Sorensen, S. M. Girvin, and A. P. Young, Phys. Rev. B **49**, 12115 (1994).
[40] M. N. Barber, in *Phase Transitions and Critical Phenomena*, edited by C. Domb and J. L. Lebowitz (Academic, New York, 1983), Vol. 8, pp. 145–266.
[41] F. Cooper, B. Freedman, and D. Preston, Nucl. Phys. B **210**, 210 (1982).
[42] J. K. Kim, Phys. Rev. Lett. **70**, 1735 (1993).
[43] S. Caracciolo, A. Gambassi, M. Gubinelli, and A. Pelissetto, Eur. Phys. J. B **20**, 255 (2001).
[44] T. Vojta and J. A. Hoyos, Phys. Rev. Lett. **112**, 075702 (2014).
[45] M. Guo, R. N. Bhatt, and D. A. Huse, Phys. Rev. Lett. **72**, 4137 (1994).
[46] H. Rieger and A. P. Young, Phys. Rev. Lett. **72**, 4141 (1994).
[47] R. Sknepnek, T. Vojta, and M. Vojta, Phys. Rev. Lett. **93**, 097201 (2004).
[48] S. Teitel and C. Jayaprakash, Phys. Rev. B **27**, 598 (1983).
[49] N. Metropolis, A. Rosenbluth, M. Rosenbluth, and A. Teller, J. Chem. Phys. **21**, 1087 (1953).
[50] U. Wolff, Phys. Rev. Lett. **62**, 361 (1989).
[51] H. G. Ballesteros, L. A. Fernández, V. Martín-Mayor, A. Muñoz Sudupe, G. Parisi, and J. J. Ruiz-Lorenzo, Phys. Rev. B **58**, 2740 (1998).
[52] H. G. Ballesteros, L. A. Fernandez, V. Martin-Mayor, A. Munoz Sudupe, G. Parisi, and J. J. Ruiz-Lorenzo, Nucl. Phys. B **512**, 681 (1998).
[53] Q. Zhu, X. Wan, R. Narayanan, J. A. Hoyos, and T. Vojta, Phys. Rev. B **91**, 224201 (2015).
[54] T. Vojta and J. Schmalian, Phys. Rev. Lett. **95**, 237206 (2005).
[55] J. Wang, Z. Zhou, W. Zhang, T. M. Garoni, and Y. Deng, Phys. Rev. E **87**, 052107 (2014).
[56] X. Xu, J. Wang, J.-P. Lv, and Y. Deng, Front. Phys. **9**, 113 (2014).
[57] D. Stauffer and A. Aharony, *Introduction to Percolation Theory* (CRC, Boca Raton, FL, 1991).